Available online at www.sciencedirect.com
SCIENCE DIRECT®
Thermochimica Acta 419 (2004) 149–159
thermochimica acta
www.elsevier.com/locate/tca

# Thermal decomposition of precursors and physicochemical characteristics of titania supported vanadia catalysts

Lori Nalbandian [a,*], Angeliki A. Lemonidou [b]

[a] *Chemical Process Engineering Research Institute, CERTH/CPERI, P.O. Box 361, 57001 Thermi, Thessaloniki, Greece*
[b] *Department of Chemical Engineering, Aristotle University of Thessaloniki and CERTH/CPERI, P.O. Box 1517, 54006 Thessaloniki, Greece*

Received 13 November 2003; received in revised form 18 February 2004; accepted 20 February 2004

Available online 9 April 2004

**Abstract**

Titania supported vanadia catalysts (2.5, 5, and 11 wt.% $V_2O_5$) were prepared by a wet impregnation technique and their thermal behavior, morphology as well as redox properties were examined by thermal analysis methods thermogravimetry (TGA), differential scanning calorimetry (DSC), temperature programmed-evolved gas analysis with mass spectroscopy, (EGA-MS), scanning electron microscopy (SEM), and temperature programmed reduction (TPR). The two Eurocat samples EL10V1 and EL10V8 containing 1 and 8 wt.% $V_2O_5$ were also characterized using the same techniques. Thermal decomposition of vanadium oxide precursors (ammonium vanadyl oxalate) supported on $TiO_2$ as evidenced by thermal analysis, occurs in three successive steps, which are influenced by the surrounding atmosphere (oxidative, reductive, and inert). The presence of tower-like vanadia crystals in the sample with the highest vanadia loading (11 wt.% $V_2O_5$) was identified by SEM. The $H_2$–TPR experiments revealed that the reduction temperature is a factor of the vanadia loading and the type of support. Vanadia species supported on Norton titania are more reducible that those supported on Eurocat titania.


*Keywords:* Vanadia catalysts; Titania; Thermogravimetry; Temperature programmed reduction; Precursors; Eurocat catalysts

## 1. Introduction

$V_2O_5/TiO_2$ catalysts are widely used in various chemical processes, such as the selective reduction of $NO_x$ with ammonia, the production of maleic anhydride, the selective oxidation and ammoxidation of hydrocarbons etc. [1–7]. The interesting catalytic performance of vanadia catalysts have stimulated considerable research efforts on the characterisation of bulk and surface properties. Supported vanadium oxide catalysts show chemical and electronic properties which are entirely different from those for the unsupported $V_2O_5$ in solid state. The structural and reactivity characteristics of $V_2O_5$ are modified when supported on $TiO_2$ and the interaction with the support leads to a high degree of dispersion over the titanium oxide surface [8,9]. It has been shown that the structure, the surface properties as well as the performance of these catalysts is strogly influenced by their preparation method and thermal treatment [10,11].

Supported vanadium oxide catalysts can be prepared via several methods. Impregnation is the most simple and widely used technique for preparing supported vanadia catalysts. The usual precursors are ammonium metavanadate and ammonium vanadyl oxalate. Understanding of the dissociation mechanisms of the precursors during catalyst formation can provide insight and information in order to prepare catalysts with special, predetermined characteristics. Very few works have been published dealing with this issue [12,13].

There is a general consensus that up to monolayer coverage which corresponds to a $VO_x$ surface density of 7–8 $nm^{-2}$ vanadia remains in amorphous form, highly dispersed on the titania anatase surface [14]. At supramonolayer coverage, crystalline $V_2O_5$ appears as evidenced mainly by XRD, IR, and Raman studies [14–17]. The morphology of $V_2O_5$ crystals and the number of amorphous layers over which the crystals grow on titania surface is a matter of controversy in the literature. Bond and coworkers in a series of articles proposed that "towers" of paracrystalline $V_2O_5$ covering a small part of the support surface are formed at supramonolayer region [10,18,19]. Van Hengstrum et al. [20] using scanning electron microscopy (SEM) observed needle-like

* Corresponding author. Tel.: +30-2310-498142; fax: +30-2310-498131.
*E-mail address:* nalbanti@alexandros.cperi.certh.gr (L. Nalbandian).

0040-6031/$ – see front matter © 2004 Elsevier B.V. All rights reserved.
doi:10.1016/j.tca.2004.02.010

$V_2O_5$ crystallites on the surface of 7.7% $V_2O_5/TiO_2$ catalysts. On the other hand, Sanati and coworkers based on TEM results showed the occurrence of amorphous $V_2O_5$ up to five monolayer [21,22].

Since most of the target reactions are of redox type, reducibility of vanadia supported catalysts has been the subject of many research efforts. Despite of the minor discrepancies due to the differences in the experimental techniques used, there is an agreement that vanadia phase is more easily reduced at low loadings corresponding to less than a monolayer than at supramonolayer content of vanadia [7,16,23–25].

Systematic characterisation of vanadia titania system was provided by a work of the European group "Eurocat-oxide" headed by Vedrine [26] in which selected samples of Eurocat samples were studied by several research laboratories.

The objective of this work was to study the mechanism of thermal decomposition of the vanadium oxide precursors during their deposition on $TiO_2$ anatase carriers. The effect of vanadia content (2.5–11 wt.%) and the carrier gas (air, hydrogen, and argon) during thermal treatment were examined. The morphology and reducibility of the prepared catalyst samples was also studied and the results were compared with the corresponding results obtained with the standard Eurocat catalyst samples.

## 2. Experimental

### 2.1. Catalyst preparation

The carrier used in all the preparations was $TiO_2$ (Norton) with particle size 100–180 μm. Catalyst samples NTiV*x*, with nominal $V_2O_5$ content 2.5 (NTiV2.5), 5 (NTiV5), and 11 wt.% (NTiV11) were prepared with the wet impregnation method. The carrier was mixed with aqueous solutions of $NH_4VO_3$ and oxalic acid, in molar ratio 1:2, and the mixture was continuously stirred at 80 °C for 2 h. The impregnated samples were dried at 120 °C for 18 h and calcined in synthetic air at 480 °C for 4 h. Samples of the unsupported complex which is formed by mixing $NH_4VO_3$ and oxalic acid solutions, stirring, evaporation, and drying were also prepared and tested with the same procedures.

The standard $V_2O_5/TiO_2$ catalyst samples, EL10V1, and EL10V8, with nominal vanadia content 1 and 8 wt.%, respectively, as well as the carrier EL10, were obtained from the Eurocat 1994 interlaboratory test. These samples already calcined (450 °C, 4 h, in air) were characterized without any further treatment.

### 2.2. Catalyst characterization

The vanadium content of all samples was measured by inductively coupled plasma-atomic emission spectroscopy (ICP-AES) with a Perkin-Elmer Plasma 40 instrument. Surface areas were determined by $N_2$ adsorption at 77 K using the multipoint BET analysis method, at a Quantachrome Autosorb-1 apparatus. Prior to the measurements, the samples were dehydrated in vacuum at 250 °C overnight. The crystalline structure of the samples was studied by XRD analysis with a Siemens D-500 diffractometer using Cu Kα radiation. The morphological characteristics of the calcined samples were examined by scanning electron microscopy (SEM, JEOL 6300) coupled with X-ray energy dispersive spectroscopy (X-ray EDS, Oxford Link ISIS-2000) for local elemental compositions determination.

Thermal analysis was performed by two different methods, thermogravimetry accompanied by differential scanning calorimetry (TGA–DSC) and temperature programmed-evolved gas analysis with mass spectroscopy (EGA-MS). TGA-DSC measurements were performed at a SDT2956 (TA instruments) thermobalance, capable to accept different types of gases as carriers (e.g. Air, Ar, $H_2$). Hydrogen was introduced as a carrier gas always mixed with Ar, at 5% $H_2$/Ar mixtures. All the measurements presented in this article were performed at constant heating rate of 10 °C $min^{-1}$.

Temperature programmed-evolved gas analysis with mass spectroscopy (EGA-MS) experiments were performed at an Altamira AMI-1 instrument equipped with a U-shaped quartz micro-reactor, heated in a vertical furnace. An on-line mass spectrometer (Omnistar Balzers) was used as the detector. For the thermal decomposition studies, typically 0.05 g sample was placed in the reactor and heated at constant rate (10 °C $min^{-1}$) from 30 to 700 °C, without any pretreatment.

Temperature programmed reduction (TPR) measurements were conducted at the above described AMI-1 instrument, coupled to the MS detector. Typically ∼0.1 g samples were placed in the reactor and preheated under Ar flow (50 ml $min^{-1}$) in order to remove any adsorbed species. After cooling down to 30 °C in flowing Ar, a TPR was carried out using 2% $H_2$/Ar mixture (50 ml $min^{-1}$), at a heating rate of 10 °C $min^{-1}$, from 30 to 700 °C. The evolution of the effluent gases was continuously monitored by the on-line mass spectrometer. In order to calibrate the MS response to $H_2$ and to account for day-to-day changes in the sensitivity of the detector, a series of 10 constant volume pulses of a 2% $H_2$/Ar mixture was performed after every TPR run.

## 3. Results and discussion

### 3.1. Catalyst precursors

#### 3.1.1. Thermal decomposition of the unsupported ammonium vanadyl oxalate

The product of mixing $NH_4VO_3$ and oxalic acid in aqueous solution is the complex compound $(NH_4)_2[VO(C_2O_4)_2]$ [12,13], which crystallizes with two $H_2O$ molecules. TGA–DSC study of the dried complex was performed in air, Ar, and $H_2$ atmospheres with a heating rate of 10 °C $min^{-1}$. The decomposition profiles are depicted in Fig. 1. It is clear that irrespective of the atmosphere, the weight loss pattern does not change up to 400 °C. The weight loss occurs in

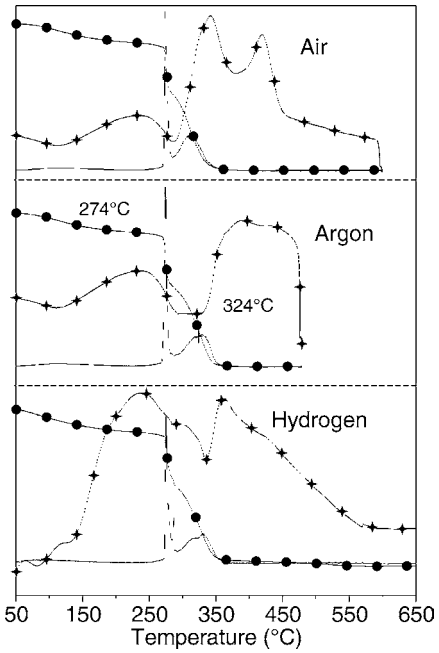


Fig. 1. Thermal decomposition profiles of the unsupported ammonium vanadyl oxalate complex under three different atmospheres: (●), TG line; (—), DTG line; and ✦, DSC line).

three successive steps. In the first step up to 200 °C crystalline water is removed corresponding to a weight loss of 9–11%. After a plateau of 70 °C, the decomposition of the ammonium vanadyl oxalate takes place in the temperature range between 270 and 370 °C amounting to 64% loss, when thermal treatment is conducted in the presence of argon and hydrogen (Fig. 1). This corresponds to the formation of $VO_2$, without any change in the valence of vanadium ($V^{4+}$). In the presence of air, the weight loss is slightly lower 61% due to oxidation $V^{4+}$ to $V^{5+}$ and subsequent formation of $V_2O_5$ (Fig. 1). In hydrogen atmosphere, a further decrease of sample weight (TG curve) is observed at the higher temperatures 450–600 °C. This is attributed to further reduction of $V^{4+}$ to $V^{3+}$.

Heat flows during decomposition in various gas atmospheres are also presented in Fig. 1. It was observed that, in the presence of $H_2$ and Ar, the weight losses are accompanied by strong endothermic effects. The findings of the present work are not in-line with those published by Bond and Flamerz [12] who reported that decomposition in the presence of $H_2$ is mildly exothermic. In the presence of oxidising carrier gas (air) the endothermic decomposition occurs simultaneously with the exothermic oxidation of $V^{4+}$ to $V^{5+}$ resulting in an initially endothermic, followed by an exothermic peak.

Evolved gas analysis, as monitored by the MS detector, revealed that the predominant gases evolved during the decomposition of the complex in the temperature region 270–370 °C, are $CO_2$, CO, $NH_3$, and $H_2O$, under the different atmospheres tested. Depending on the carrier gas, differences were observed in the relative concentration of the

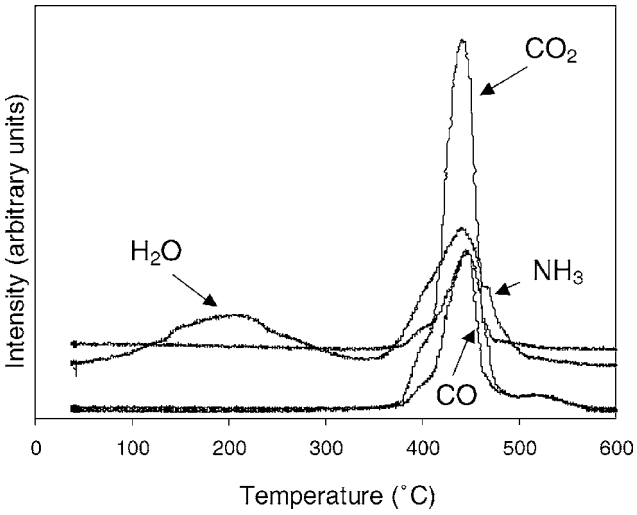


Fig. 2. Evolved gas as detected by the MS detector during the thermal decomposition of the unsupported ammonium vanadyl complex in the presence of air.

evolved gases, the most important of which is the $CO_2$/CO ratio.This ratio attained the highest value in the presence of air. Fig. 2 shows the evolved gases during temperature programmed heating of the unsupported complex in the presence of air.

### 3.1.2. Thermal decomposition of precursors supported on $TiO_2$ carrier

Uncalcined samples with different V loadings, as well as the pure support NTi, where studied with thermal analysis methods (TGA–DSC) under oxidative, inert, and reductive atmospheres. A weight loss of 1.2% was observed for the support when heated in air or Ar between 600 and 800 °C (not shown). This would be ascribed to removal of adsorbed molecular water and hydroxyl groups.

The decomposition curves (heat flow, weight loss, and derivative weight) obtained in the presence of the three different carrier gases (air, argon and hydrogen) for sample NTiV11 is presented in Fig. 3. In contrast with the unsupported, the decomposition temperature of the supported precursor is affected by the carrier gas. The main decomposition of the NTiV11 sample occurs in 212 °C in the presence of air, while significantly higher temperature (312 °C) is needed for the decomposition in the presence of argon (Fig. 3). Almost the same decomposition temperatures are observed with NTiV5 sample (Fig. 4) and NTiV2.5 (not shown) indicating that the concentration of vanadia precursor on the support surface is not a critical factor. Furthermore, from the above figures, it can be inferred that the decomposition of the precursor occurs during three successive steps (first: 211 °C, second: 311 °C, and third: 425 °C), the relative significance of each of them being determined by the surrounding atmosphere. For comparison it should be mentioned here that the decomposition of the unsupported complex occurs in a temperature range very close to that of the second step (see Fig. 1).

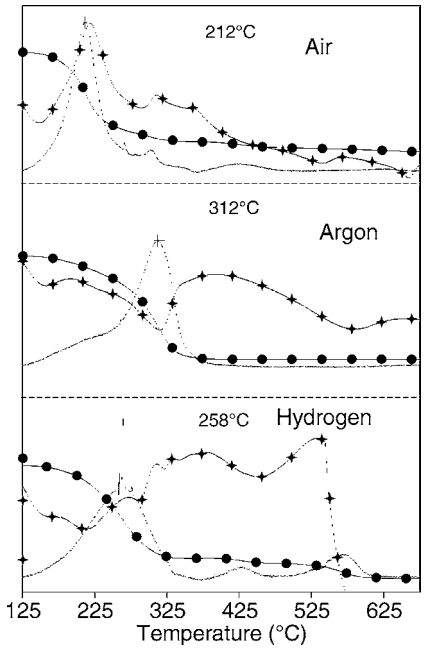


Fig. 3. Thermal decomposition profiles of the uncalcined sample NTiV11 (11 wt.% $V_2O_5$), under different gas atmospheres: (●), TG line; (—), DTG line; and ✦, DSC line.

Under flowing air, more than 90% of the decomposition of NTiV11 and NTiV5 precursors takes place during the first step (DTG peak: 211 °C) accompanied by a strong exothermic effect. Significantly smaller weight losses are observed in the two consecutive steps occuring at higher temperatures (311 and 425 °C), which are also exothermic.

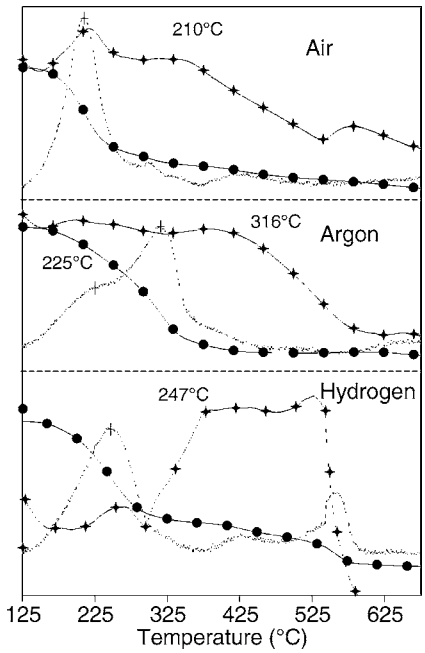


Fig. 4. Thermal decomposition profiles of the uncalcined sample NTiV5 (5 wt.% $V_2O_5$), under different gas atmospheres: (●), TG line; (—), DTG line; and ✦, DSC line.

In Ar flow more than 80% of the decomposition of NTiV11 sample occurs during the second, medium temperature, step accompanied by a strong endothermic peak. The decomposition of NTiV5 proceeds via the same steps but the relative significance of the first step increases. As shown in both Figs. 3 and 4 the third step is absent when the precursor decomposition occurs in the presence of Ar.

In the presence of $H_2$ the first two steps are merged in one unresolved DTG peak at an intermediate temperature (DTG peak: 266 °C) accompanied by two endothermic DSC peaks. In the same manner as with Ar, lower V content (5 wt.%) results in an increase of the significance of the first step, as demonstrated by the shift of the DTG peak from 258 to 246 °C (compare Figs. 3 and 4). The temperature differences observed during the decomposition of the supported precursor are in agreement with the results of the corresponding study for the Eurocat samples [27] where decomposition in air and argon atmospheres were performed.

The differences observed in the decomposition temperature suggest that, while the inert Ar does not participate in the decomposition of the precursor, the presence of both the reductive $H_2$ and the oxidative $O_2$, facilitates the decomposition reactions. The promoting effect of $H_2$ and air (oxygen) in the presence of the titania may be due to the adsorption and activation of these gases on the titania surface faciliting thus the decomposition of the adsorbed vanadyl complex. The decomposition reaction is endothermic, however, in the presence of oxidizing air atmosphere the strongly exothermic oxidation of $V^{4+}$ to $V^{5+}$ occuring simultaneously changes the sign of the whole effect.

Based on the measured weight loss during heating of the uncalcined samples with different V loadings, the molecular weight of the supported precursor was calculated at MW $\cong$ 189 $\pm$ 8. The values of MW calculated from the weight loss curves under the various gas atmospheres and V loadings were in very good agreement. Given that the molecular weight of free ammonium vanadyl oxalate is 315, it is clear that the complex formed in the presence of titania support has a different molecular formula. We propose that the molecular formula of the precursor supported on $TiO_2$ is $(NH_4)[VO(C_2O_4)]$–O–S (S = support). The proposed formula is in agreement with Weckhuysen and Keller [11] who reported that the interaction of the ionic oxalate complex with the support proceeds via an exchange reaction and ligand substitution (exchange of ligands of the metal complex for functional groups of the support oxides). This results in a complex with different molecular structure than this of the complex in the absense of a supporting material.

### 3.2. Catalysts

#### 3.2.1. Physicochemical characterization of calcined catalysts

The composition and the physicochemical characteristics of the prepared calcined catalysts and the Eurocat catalysts are presented in Table 1 and Figs. 5 and 6.

Table 1
Physicochemical characteristics of catalyst samples

| Sample | V content (ICP), g $V_2O_5$ per 100 g sample | BET surface area, ($m^2\ g^{-1}$) | $VO_x$ density (V atoms per square nanometre) |
|---|---|---|---|
| NTi (carrier) | – | 49.9 | – |
| NTiV2.5 | 2.72 | 44.5 | 4.0 |
| NTiV5 | 4.94 | 43.0 | 7.6 |
| NTiV11 | 11.27 | 29.1 | 25.6 |
| EL10 (carrier) | – | 14.62 | – |
| EL10–V1 | 1.02 | 13.82 | 4.89 |
| EL10–V8 | 7.9 | 14.92 | 35.05 |

The XRD diffractograms of the samples show (Fig. 5) that with NTiV2.5 and NTiV5 samples, as well as with EL10V1 sample (Fig. 6), the only peaks detected are those characteristic of the titania anatase support suggesting that vanadia species are well dispersed on the support. Peaks of crystalline $V_2O_5$ appear in the diffractograms of NTiV11 and EL10V8 samples with high vanadia loadings in agreement with previous studies [2,14,26] for catalysts with $VO_x$ density above monolayer.

The anatase XRD peaks obtained with NTi Norton titania are much broader than the corresponding peaks obtained with EL10 Eurocat titania as clearly shown in Figs. 5 and 6, respectively. The mean crystallite size of the NTi titania (≅40 nm) was found to be much smaller than the mean crystallite size of the EL10 titania (≅200 nm) by applying Scherrer analysis to the X-ray diffactograms.

The surface areas of the NTiV*x* samples are significantly affected by the V content as shown in Table 1. Vanadia addition reduces the surface area of the NTi carrier (50.5 $m^2\ g^{-1}$) by extent analogous to the V content. The surface area of the Eurocat samples is practically not affected by the vanadia loading most probably due to the significantly lower surface area of the EL10 carrier.

The model for spherical non-porous particles was applied to the two carriers NTi and EL10 in order to calculate the external surface area that corresponds to the mean particle size as predicted from the XRD Scherrer analysis (40 and 200 nm, respectively). The values obtained are very close to the measured BET surface areas of the two carriers, concluding that all the surface area of the samples is due to the external surface area of their particles and not to internal porosity.

The morphology of all prepared samples was studied by electron microscopy. The images of the two carriers NTi and EL10, presented in Fig. 7a and b, show clearly the difference in the crystallite sizes. NTi titania has crystallites with sizes ranging from 30 to 60 nm while EL10 titania has significantly larger crystallites (100–250 nm). These values fully agree with the predictions of the XRD Scherrer analysis and $N_2$ sorption measurements.

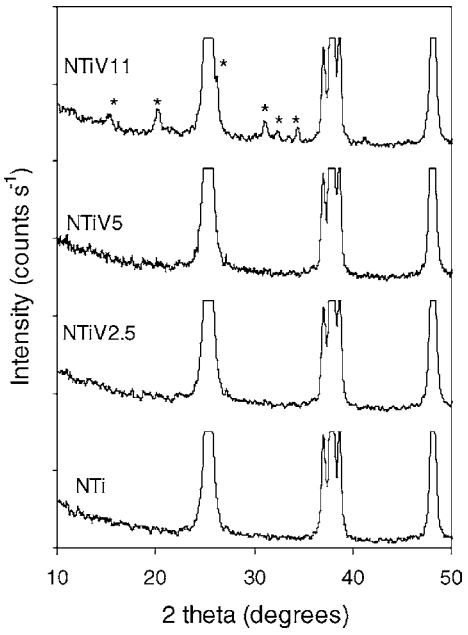


Fig. 5. X-ray diffractograms of the pure Norton titania support and the supported vanadia catalysts NTiV*x* (2.5–11 wt.% $V_2O_5$).

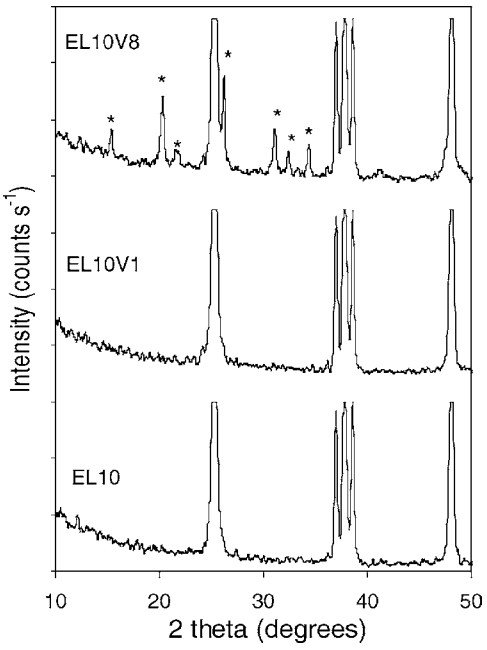


Fig. 6. X-ray diffractograms of the EL10 pure support and the Eurocat catalysts.

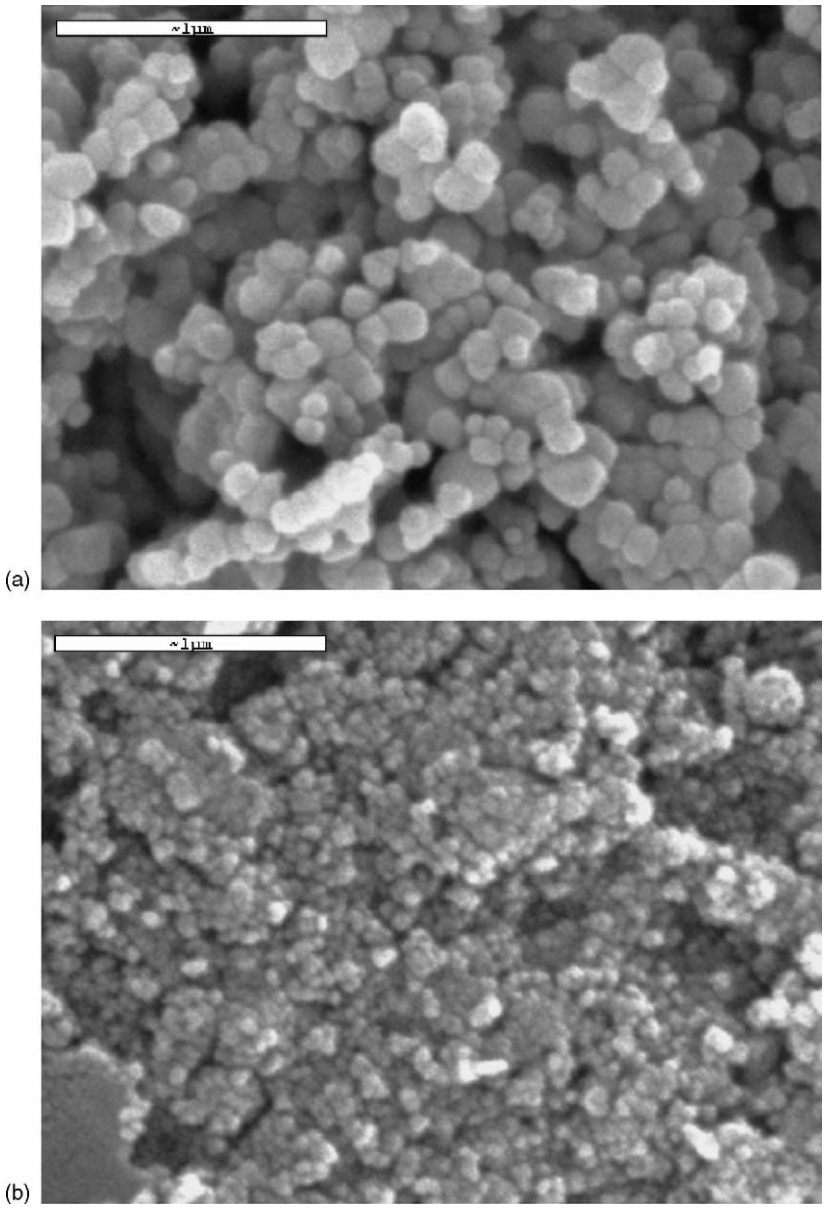


Fig. 7. SEM images of the Eurocat (a) and Norton (b) catalyst carriers.

The images obtained with samples NTiV2.5 and NTiV5 are practically the same as those obtained with the NTi carrier (not shown). This is not surprising since there is no indication from the other experimental techniques employed that different features (at the length scale observable by SEM) would exist on the surface. EDS analysis of the above samples showed that V is evenly distributed over the titania carrier. The Eurocat samples (EL10V1 and EL10V8) also do not present any features different from the EL10 pure support. Previous studies of these samples have shown that the $V_2O_5$ crystallites detected by XRD in the EL10V8 sample cannot be observed by SEM. The $V_2O_5$ crystallites as observed on the surface of EL10V8 samples by HREM [28], have irregular platelet-like shapes with dimensions of approximately $25 \times 120$ nm. However, the image of NTiV11 sample is quite different. Besides the already known $TiO_2$ anatase crystallites, the existence of needle crystals is detected (Fig. 8a and b), which cover a relatively small fraction of the support surface. The formation of tower-like crystallites of $V_2O_5$ over the vanadia monolayer has been already theoretically predicted by Bond et al. [18,19], based on XPS measurements. They interpreted XPS results as being caused by the occurrence of "towers" of the "disordered" and "paracrystalline" $V_2O_5$, formed on the monolayer. They claimed that these "towers" ultimately become needle-like growths of $V_2O_5$, growing away from the surface, but being distinctly more easily reduced than normal $V_2O_5$. The occurence of the $V_2O_5$ needles has also been observed by SEM from van Hengstrum et al. [20]. They reported that at high loadings, crystalline $V_2O_5$

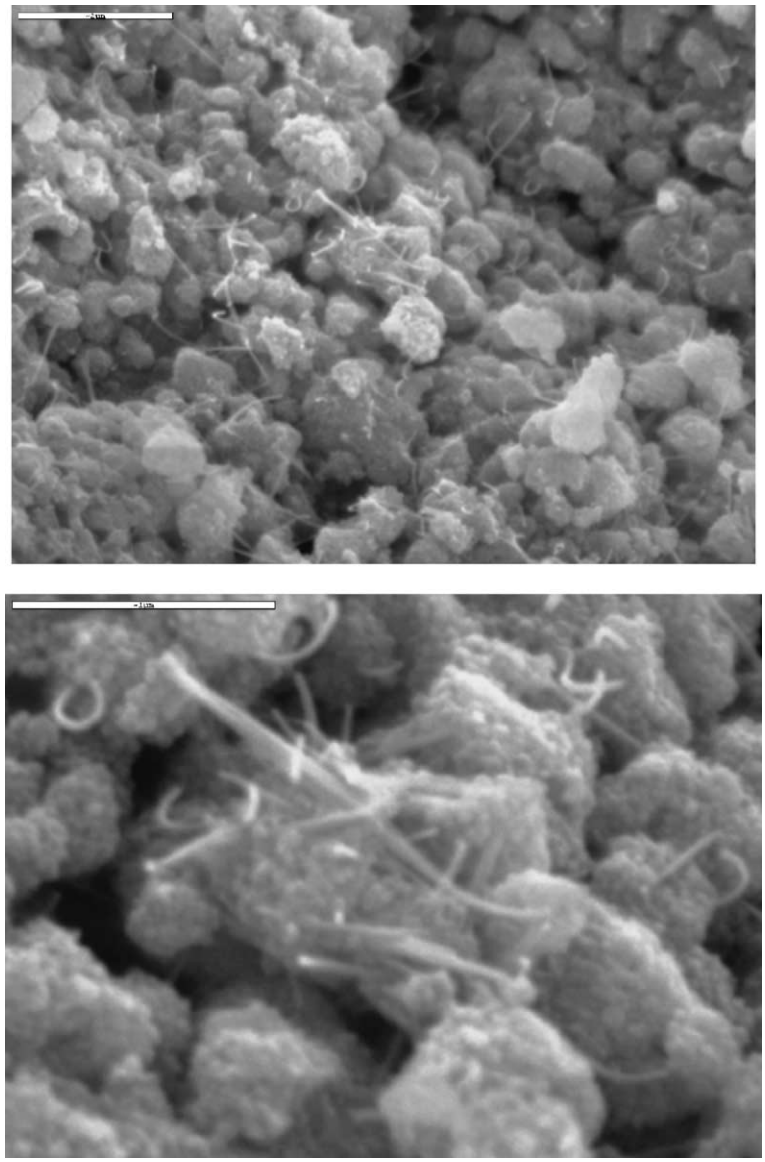

Fig. 8. SEM images of catalyst NTiV11 (11 wt.% $V_2O_5$).

needles are formed, which do not influence the catalyst behavior.

In order to clarify whether the occurrence of the $V_2O_5$ needle crystals is due to the support type or to the preparation method a new sample was prepared with 5.4 wt.% $V_2O_5$ supported on the EL10 carrier. The procedure used for the preparation was the same as with the NTiV*x* samples. The $V_2O_5$ content was selected so as to have the same theoretical $VO_x$ density as the NTiV11 sample. The morphology of the particles of the above mixed type sample was observed by electron microscopy. Fig. 9 shows that no indication for formation of needle crystals exists. On the contrary, smooth particles with sizes ranging from 100 to 250 nm are clearly visible of the same morphology as those observed with the other Eurocat samples. It is thus concluded that the growth of $V_2O_5$ needle crystals is closely connected to the specific type of the NTi support. Based on the above findings it seems that the disagreement in the literature about the $V_2O_5$ crystals morphology above monolayer coverage can be resolved since both reported cases are possible.

### *3.2.2. Temperature programmed reduction of V oxides*

The reducibility of the supported V oxides was studied by measuring the weight loss of the samples (TGA) during heating under flowing $H_2$, and by monitoring the decrease of the concentration of an $H_2$ stream, with simultaneus measurement of the evolved gas during reduction (TPR–EGA). The results obtained with the two techniques are in very good agreement both qualitatively, in temperature determination, and quantitatively, in degree of reduction. As will be shown below, TGA has better resolution than the TPR–EGA, in distinguishing reduction peaks at adjacent temperatures.

Fig. 10 presents the TPR profiles of the NTiV*x* samples. In TPR–EGA curves (Fig. 10a), samples NTiV2.5 and

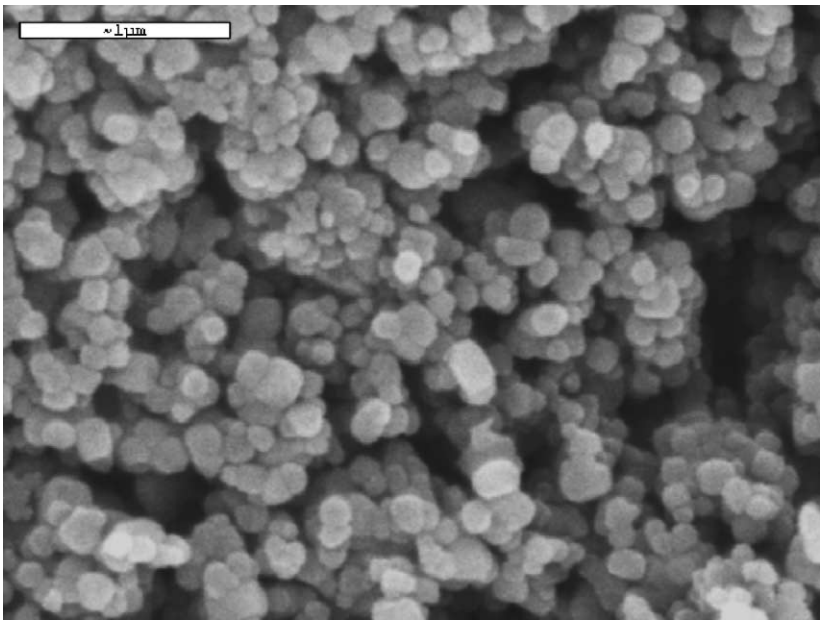


Fig. 9. SEM image of the mixed type catalyst 5.4 wt.% $V_2O_5$ on Eurocat carrier prepared with the methods of this work.

NTiV5, in which V exists only in a monolayer, show only one broad peak in the region 500–600 °C, which is attributed to the reduction of vanadia species. The $T_{max}$ (temperature at maximum $H_2$ consumption rate) of NTiV5 (547 °C) is slightly higher than that of the NTiV2.5 sample (531 °C). In the TGA–$H_2$ curves (Fig. 10b), which as already mentioned have better resolution, two, instead of one, peaks appear for both samples ($T_{max}$, 526 and 562 °C). The two peaks could be ascribed to the differences in the reducibility of the different types of $VO_x$ species existing on the surface. The shift of the TPR peak maximum to higher temperatures with increasing V content is more clearly shown in the TGA curves. The ratio of the low to high temperature peak intensities decreases from NTiV2.5 to NTiV5 sample, indicating different population of the various types of $VO_x$ features. Previous Raman studies [14–17], have shown that in samples with less than monolayer coverage, mono- and polyvanadate $VO_x$ species are present and that their relative concentration varies significantly with V content. From the results of the TPR and TGA–$H_2$ study one cannot conclude about the nature of the $VO_x$ species present, since there are controversial results in the literature [24,29] about their relative reducibility.

The TPR–EGA profile of NTiV11 sample with supramonolayer $VO_x$ coverage (Fig. 10a) is a broad curve, with the same onset temperature as those of the previous samples, extending to considerably higher temperatures with $T_{max}$ at 596 °C. The TGA–$H_2$ curve of NTiV11 (Fig. 10b) presents the same features as the TPR–EGA curve with $T_{max}$ at 598 °C. The observed broad band can be analyzed into three unresolved peaks, the first two of which coincide with the two peaks observed with the low V samples. Those low tempearure peaks may be attributed to $VO_x$ species co-existing on the catalyst surface, which reduce in different steps. The same $T_{onset}$ clearly suggests that the same type of easily reducible V species coexist on the surface of the three catalysts. The predominant peak has maximum at significantly higher temperature than the NTiV2.5 and NTiV5 samples. TPR experiments with bulk $V_2O_5$ showed that the reduction of the pure crystalline species (not shown) starts at temperatures higher than 620 °C, in agreement with previous works [7,16,23–25]. Thus, this new high temperature peak can be attributed to the reduction of crystalline vanadium species, which occurs at slightly lower temperature than the unsupported crystal $V_2O_5$ due to the interaction with the support [23].

Fig. 11 presents the TPR results obtained with Eurocat samples. Both TGA–$H_2$ and TPR–EGA curves show that reduction of $VO_x$ species occurs in the temperature region 500–700 °C. Sample EL10V1, with V content close to monolayer, presents one reduction peak at 574 °C. Sample EL10V8, with V content corresponding to approximately eight monolayers has two, clearly resolved, reduction peaks, as measured by both methods. The difference in relative intensities of the two peaks measured by the different techniques can be attributed to the higher resolution of the TGA–$H_2$ method. The second, high temperature, peak of the EL10V8 sample can be ascribed to the reduction of the crystalline $V_2O_5$, the presence of which has been identified by XRD, similarly as with the high temperature peak of the NTiV11 sample. The better resolution of the low and high temperature peaks obtained with the EL10V8 sample, as compared to the broad unresolved reduction curve of NTiV11 sample, is most probably due to the higher content of crystalline $V_2O_5$ in the EL10V8 sample (equivalent to eight monolayers) compared to NTiV11 sample (equivalent to three monolayers).

By comparing the reduction profiles as presented in Figs. 10 and 11 it is clear that the reduction temperature of

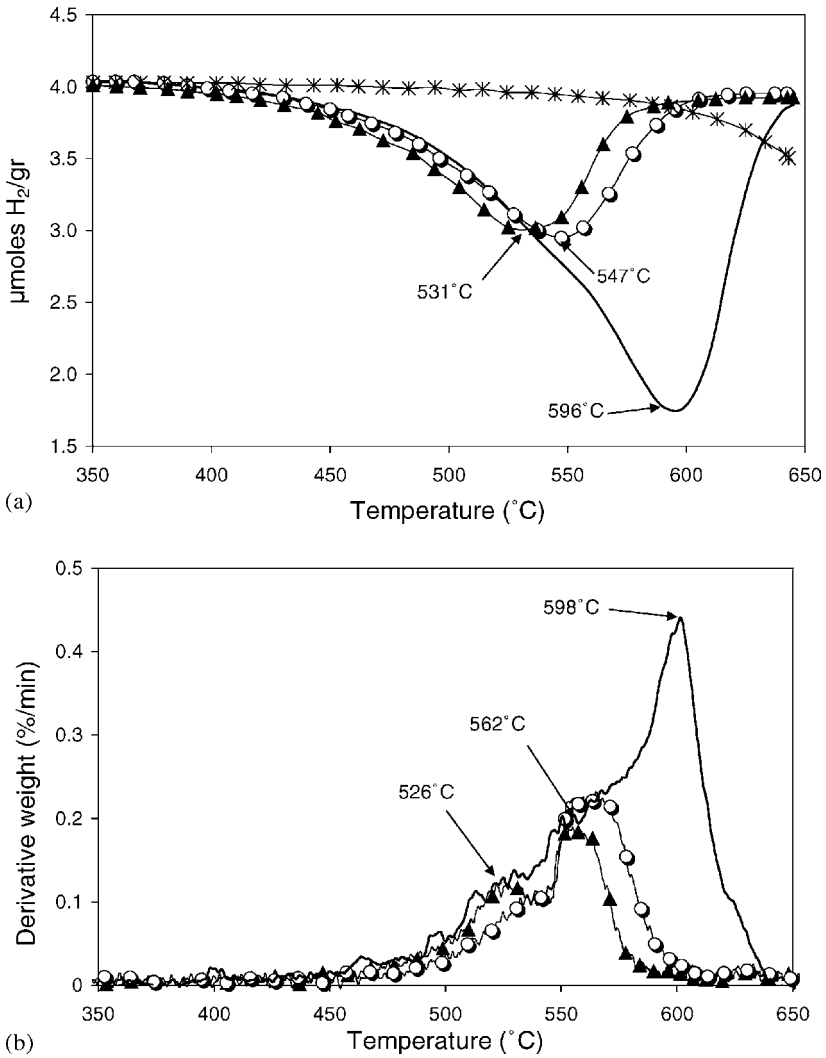


Fig. 10. $H_2$–temperature programmed reduction of NTiV*x* supported vanadia catalysts and the NTi support (a) TPR–EGA: (—), NTiV11; (○), NTiV5; (▲), NTiV2.5; and ✳, NTi. (b) TGA–$H_2$ (DTG curves): (—), NTiV11; (○), NTiV5; (▲), NTiV2.5.

NTiV*x* samples is considerably lower than that of Eurocat samples. More specifically the difference in the reduction temperature of monolayer and sub-monolayer samples is approximately 50 °C, while the difference for the samples with supramonolayer coverage is even higher (∼60 °C).

Apart from the different acidity [30] other properties of the two supports may account for the differences obtained in reduction profiles. The presence of the impurities in the pigment grade Eurocat support and more precisely of K and P may hinder the reducibility of the Eurocat catalyst. XRF and XPS measurements showed that titania has a large number of impurities with more significant those of K and P oxides [26]. It is well known that the above mentioned elements even in small amounts shift the temperature of maximum hydrogen consumption [4,31]. Furthermore, based on the characterization presented above, there are also other differences between the two titanias used in this study; different crystallite size and different degree of reduction. Both characteristics could affect the reduction temperature of the catalysts. As shown before, both carriers have no internal porosity, all their surface area being at the external surface of their particles. It is thus reasonable to assume that vanadia monolayer is formed around the carrier crystallites. The bigger the crystallite, the more uniform, without discontinuities the monolayer should be. When the monolayer is formed around small particles, the occurence of discontinuities and grain boundaries cannot be excluded. Since the reduction of $V_2O_5$ in the monolayer is a temperature activated process, the presence of the above defect points at the monolayer surface could initiate the reduction, by overcoming the energy barrier which is otherwise necessary. Furthermore, the reduction of $VO_x$ species over the NTi carrier could also be facilitated by the reduction of the titania carrier itself. In Figs. 10a and 11 the TPR curves of the two titania carriers NTi and EL10 are shown, together with the TPR curves of the catalyst samples. NTi titania shows a low intensity reduction peak with onset temperature below 650 °C, while EL10 titania does not show any reduction in the temperature

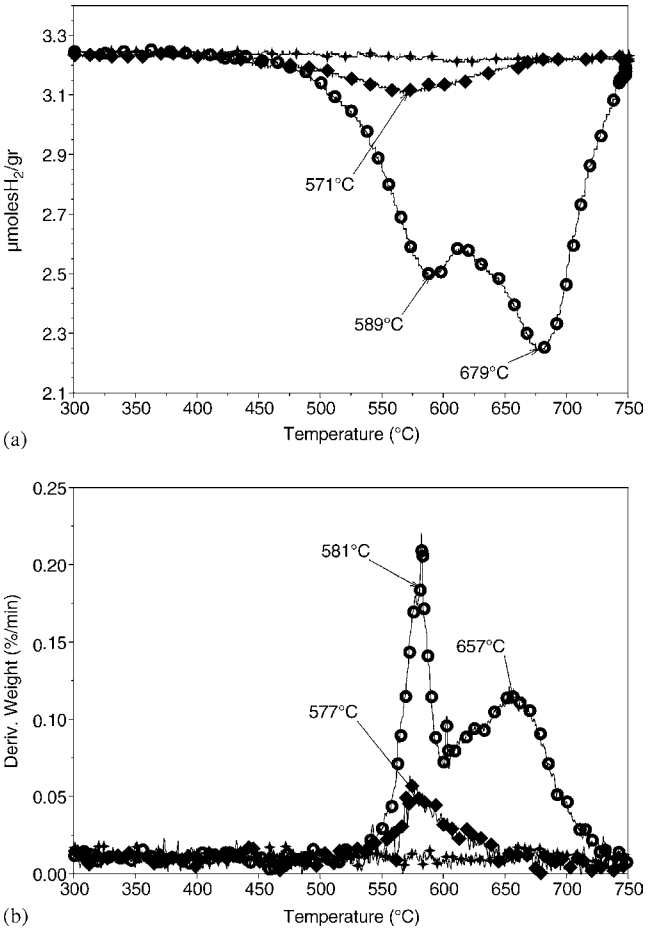


Fig. 11. $H_2$-temperature programmed reduction of Eurocat 1994 catalysts and the EL10 carrier (a)TPR–EGA: (+), EL10; (◆), EL10V1; and (○), EL10V8. (b) TGA–$H_2$ (DTG curves): (+), EL10; (◆), EL10V1; and (○), EL10V8.

range up to 750 °C. No sign of reduction at 650 °C appears in the TPR profiles of all NTiV*x* catalysts indicating that the reduction of $VO_x$ species is at the same time facilitating and facilitated by the reduction of the titania support. This may account for the enhanced reducibility of V species in lower than monolayer coverage supported on NTi, over those supported on EL10 titania. Reduction of titania has been reported in literature [32–34]. The same Norton titania, as the one used in this work, was used as support for Mo catalysts by Maity et al. [32]. During TPR studies the above researchers mentioned that their pure support was reduced at temperature approximately 740 °C, but its reduction temperature was shifted to 620 °C upon the addition of 2 wt.% Mo.

The integrated hydrogen consumption, as calculated from TGA–$H_2$ and TPR–EGA, are presented in Table 2. For the Eurocat samples, EL10V8 and EL10V1, both, the weight loss in the temperature range of the reduction obtained from TGA–$H_2$ measurements and the integrated hydrogen consumption calculated from the TPR curves correspond to complete reduction of V from +5 to +3. These results are in perfect agreement with previous studies concerning the Eurocat samples [23,26].

The results obtained from the NTiV*x* samples are not straightforward interpretable. The weight loss and $H_2$ consumption for the NTiV11 sample matches to the $V^{5+}$ to $V^{3+}$ transition. However, when the V content is close or less than monolayer, much higher than the theoretical weight loss and corresponding $H_2$ consumption are measured, especially for the NTiV2.5 sample. The above discrepancy can be interpreted by taking into account the fact that in the samples with coverages less than a monolayer, there is still free titania surface which can be reduced, as described above. The $T_{max}$ for the reduction of the above free titania decreases

Table 2
Experimental and calculated data for $V_2O_5$ reduction with the TGA–$H_2$ and TPR–EGA–$H_2$ methods

| Catalyst | $V_2O_5$ (%) | Measured weight loss (%) | Theoretical weight loss due to $V^{5+} \rightarrow V^{3+}$ reduction | Weight loss due to $TiO_2$ free surface reduction |
|---|---|---|---|---|
| TGA–$H_2$ | | | | |
| NTi | 0 | 1.57 ± 0.1 | 0 | 1.57 ± 0.1 |
| NTiV2.5 | 2.72 | 1.09 ± 0.1 | 0.48 | 0.61 ± 0.1 |
| NTiV5 | 4.94 | 1.12 ± 0.1 | 0.87 | 0.25 ± 0.1 |
| NTiV11 | 11.27 | 1.96 ± 0.1 | 1.98 | −0.02 ± 0.1 |
| EL10V8 | 7.9 | 1.42 ± 0.1 | 1.39 | 0.03 ± 0.1 |
| EL10V1 | 1.02 | 0.24 ± 0.1 | 0.18 | 0.06 ± 0.1 |
| EL10 | 0 | 0 | 0 | 0 |
| Catalyst | $V_2O_5$ (%) | $H_2$ consumed ($\mu mol\,g^{-1}$) | Theoretical $H_2$ consumption due to $V^{5+} \rightarrow V^{3+}$ reduction | $H_2$ consumption due to $TiO_2$ free surface reduction |
| TPR–EGA–$H_2$ | | | | |
| NTi | 0 | 600 ± 40 | 0 | 600 ± 40 |
| NTiV2.5 | 2.72 | 503 ± 40 | 299 | 204 ± 40 |
| NTiV5 | 4.94 | 598 ± 40 | 543 | 55 ± 40 |
| NTiV11 | 11.27 | 1272 ± 40 | 1238 | 34 ± 40 |
| EL10V8 | 7.9 | 823 ± 40 | 868 | −45 ± 40 |
| EL10V1 | 1.02 | 97 ± 40 | 112 | −15 ± 40 |
| EL10 | 0 | 0 | 0 | 0 |

and is indistinguishable from the reduction peak of the $VO_x$ species of the monolayer, most probably due to the effect of the neighboring V. From the results presented in Table 2 and the hypothesis of the coexistence of reducible titania and $VO_x$ species, it was estimated that the free titania surface is approximately $35 \pm 5\%$ for the NTiV2.5 sample and around $10 \pm 5\%$ for the NTiV5 sample. It is interesting to note that the results of both techniques are in very good agreement confirming the hypothesis that part of weight loss or $H_2$ consumption is due to the reduction of free $TiO_2$ on the surface.

The above quantitative analysis has been based on the assumption that the final oxidation state of vanadium in the reduced samples is +3, in-line with most relevant works [23,24,26,31]. Nevertheless, the formation of $V^{4+}$ during the $H_2$ reduction of titania supported vanadia cannot be excluded [14]. Present results do not provide any evidence of $V^{4+}$ formation. However, even if small quantities of tetravalent vanadium was formed, this would not change the above discussion, since the reduction $V^{5+} \rightarrow V^{4+}$ results in less hydrogen consumption and less weight loss.

## 4. Conclusions

The investigation of the decomposition mechanism of ammonium vanadyl oxalate complex (vanadia precursor) supported on Norton titania by thermal analysis showed that the formation of $VO_x$ species proceeds via successive steps up to 450 °C, depending on the nature of the surrounding atmosphere. Oxidative and reductive atmospheres facilitate the decomposition of the supported complex compared to inert atmosphere.

Examination of the size of the two supports used (Norton titania and Eurocat EL10) by SEM and XRD showed that the size of Norton titania crystallites (40 nm) is much smaller that that of Eurocat (200 nm). This difference in the support crystal size may account for the observed differences in the morphology of $V_2O_5$ crystals formed on the surface of high V loading samples.

Reducibility of the vanadia catalysts in $H_2$ flow as investigated by the application of TGA and TPR techniques was found to be related to the vanadia content and the support nature. More than one reduction peaks with various intensities as evidenced especially from TGA measurements were ascribed to the different nature and population of $VO_x$ domains on the catalyst surface. The significantly lower reduction temperatures observed with the titania Norton supported catalysts compared to that of Eurocat were attributed to the different characteristics of the two supports (absence of K and P impurities, low extent reduction of Norton titania and smaller size of crystallites). Higher than the stoichiometric $H_2$ consumption or weight loss obtained with the Norton titania supported samples were ascribed to the reduction of the free titania on the surface.

## Acknowledgements

The authors greatfully acknowledge Maria Machli and Sotiria Gogaki for their help with the preparation of the catalytic samples.

## References

[1] G. Centi, F. Cavani, F. Trifiro, Selective Oxidation by Heterogeneous Catalysis, Kluwer Academic, 2001 p. 222.
[2] G. Centi, Appl. Catal. A 147 (1996) 267.
[3] H. Bosh, F.J. Janssen, Catal. Today 1 (1988) 369.
[4] G. Deo, I.E. Wachs, J. Catal. 146 (1994) 323.
[5] A.A. Lemonidou, L. Nalbandian, I.A. Vasalos, Catal. Today 61 (2000) 333.
[6] N.V. Economidis, D.A. Pena, P.G. Smirniotis, Appl. Catal. B 23 (1999) 123.
[7] B. Grzybowska-Swierkosz, Appl. Catal. A 157 (1997) 263.
[8] P. Courtine, E. Bordes, Appl. Catal. A 157 (1997) 45.
[9] G. Centi, B. Pinelli, F. Trifiro, J. Mol. Catal. 59 (1990) 221.
[10] G.C. Bond, Appl. Catal. A 157 (1997) 91.
[11] B.M. Weckhuysen, D.E. Keller, Catal. Today 78 (2003) 25.
[12] G.C. Bond, S. Flamerz, Appl. Catal. 46 (1989) 89.
[13] X.S. Li, L.Y. Chen, C.Y. Xie, Y.F. Miao, D.M. Li, Q. Xin, Thermochim. Acta 260 (1995) 115.
[14] I.E. Wachs, B.M. Weckhuysen, Appl. Catal. A 157 (1997) 67.
[15] S. Besselmann, E. Löffler, M. Muhler, J. Mol. Catal. A 162 (2000) 401.
[16] D.A. Bulushev, L. Kiwi Minsker, F. Rainone, A. Renken, J. Catal. 205 (2002) 115.
[17] A. Christodoulakis, M. Machli, A.A. Lemonidou, S. Boghosian, J. Catal. 222 (2004) 293.
[18] G.C. Bond, J. Perez Zurita, S. Flamerz, Appl. Catal. 27 (1986) 353.
[19] G.C. Bond, S.F. Tahir, Appl. Catal. 71 (1991) 1.
[20] A.J. van Hengstum, J.G. van Ommen, H. Bosch, P.J. Gellings, Appl. Catal. 8 (1983) 369.
[21] M. Sanati, L.R. Wallenberg, A. Anderson, S. Jansen, Y. Tu, J. Catal. 132 (1991) 128.
[22] L.R. Wallenberg, M. Sanati, A. Anderson, J. Catal. 126 (1990) 246.
[23] S. Besselmann, C. Freitag, O. Hinrichsen, M. Muhler, Phys. Chem. Chem. Phys. 3 (2001) 4633.
[24] G. Went, L.-J. Leu, A.T. Bell, J. Catal. 134 (1992) 479.
[25] A. Satsuma, S. Takenaka, T. Tanaka, S. Nojima, Y. Kera, H. Miyata, Appl. Catal. A 232 (2002) 93.
[26] J.C. Vedrine (Ed.), EUROCAT oxide (special issue), Catal. Today 20 (1) 1994.
[27] V. Rives, Catal. Today 20 (1994) 35.
[28] M. De Boer, Catal. Today 20 (1994) 97.
[29] X. Gao, J-M. Jehng, I.E. Wachs, J. Catal. 209 (2002) 43.
[30] M. Machli, A.A. Lemonidou, unpublished results.
[31] B. Grzybowska-Swierkosz, Top. Catal. 21 (2002) 35.
[32] S.K. Maity, M.S. Rana, S.K. Bej, J. Ancheyta-Juarez, G. Murali Dhar, T.S.R. Prasada Rao, Appl. Catal. A 205 (2001) 215.
[33] J-M. Hermann, J. Didier, G. Deo, I.E. Wachs, J. Chem. Soc.; Faraday Trans. 93 (8) (1997) 1655.
[34] X. Gao, S.R. Bare, J.L.G. Fierro, I.E. Wachs, J. Phys. Chem. B 103 (1999) 618.